Hindawi
Advances in Materials Science and Engineering
Volume 2022, Article ID 7629651, 10 pages
https://doi.org/10.1155/2022/7629651

Research Article

Ab initio Investigation of the Structural and Electronic Properties of Alkaline Earth Metal - TiO2 Natural Polymorphs

Jane Kathure Mbae and Zipporah Wanjiku Muthui

Chuka University, P.O. Box 109 60400, Chuka, Kenya

Correspondence should be addressed to Zipporah Wanjiku Muthui; ciku32ke@yahoo.com

zwanjiku@chuka.ac.ke

Received 26 January 2022; Revised 2 March 2022; Accepted 10 March 2022; Published 27 March 2022

Academic Editor: Zhongchang Wang

Copyright © 2022 Jane Kathure Mbae and Zipporah Wanjiku Muthui. This is an open access article distributed under the Creative Commons Attribution License, which permits unrestricted use, distribution, and reproduction in any medium, provided the original work is properly cited.

Titanium (IV) oxide (TiO_2) has gained much attention due to its application in technologies such as optoelectronics, electronics, sensors, photocatalysts, and sustainable energy generation. However, its optical absorption falls in the ultraviolet part of the electromagnetic spectrum, resulting in a low absorption ratio of solar light. In addition, rapid electron-hole recombination limits its photocatalytic activity. To extend the application range of TiO_2, the structural and chemical properties can be modified by adding various dopants to tune its electronic structure for applications within a wider range of the solar energy spectrum and ideally extend towards the visible region, which forms the dominant part of the solar energy spectrum. In this study, the structural and electronic properties of three polymorphs of TiO2 have been studied using density functional theory (DFT) as implemented in the Quantum ESPRESSO simulation package. The exchange-correlation potential has been treated with the generalised gradient approximation (GGA). Cationic substitution with non-toxic alkaline earth metal dopants Mg and Ca has been carried out with the aim of modifying the electronic structure of the polymorphs of TiO_2. On 1–4% Mg and Ca cationic substitution, there is a slight expansion of the optimal unit cell volume and modulation of the band gap energy by raising the valence band maximum to higher energies. In addition, dopant inter and intra-band states are observed.

1. Introduction

Transition metal oxide, titanium (IV) oxide, TiO2, also known as titania, has attracted increased research attention due to its properties such as excellent optical [1, 2], chemical, and electrical properties [2], low cost [3, 4], natural geologic abundance [5, 6], high thermal stability [5], super-hydrophilicity [2], and low toxicity [5, 6]. These properties can be exploited for advances in various technological applications such as in electronics [7], photocatalysis [2, 6, 8–11] and environmental cleanup [2, 10, 11], hydrogen production and storage [6, 7], novel solar cells [6, 11], realization of spintronic devices [12, 13], antireflection coatings and sensors [9, 12], and UV-induced electron photoexcitation in paint pigment [2, 6] and as a ferroelectric material at low pressures [12] among other applications. Others include light-induced amphiphilic surfaces and antibacterial applications [2].

Titania is a polymorphic material consisting of eleven polymorphs with the crystal structures ranging from the high symmetry cubic structure to the low symmetry monoclinic crystalline structure. The forms that occur naturally are the rutile (tetragonal, P42/mnm), anatase (tetragonal, I41/amd) and brookite (orthorhombic, Pbca) crystalline phases [2]. While the anatase phase commonly exists in TiO2 nanoscale materials [6] and is the most photoactive phase than other TiO2 polymorphs [2], rutile is the most thermodynamically stable and abundant phase [5]. TiO2 has a low efficiency for applications involving solar energy due to the wide band gap of 3.2 eV for anatase and 3.06 eV for rutile, which restricts its photocatalytic application to the ultraviolet range, utilizing only about 3–5% of total sunlight [6, 8, 14, 15]. Further, weak separation efficiency of photo-carriers results in charge recombination, which restricts the photocatalytic activity in TiO2 [8]. To overcome these limitations, techniques aimed at extending

the spectral response of TiO2 to the visible region, which accounts for approximately 40% of the solar energy spectrum, such as energy band gap modulation and better light sensitization of TiO2 have been undertaken [3, 5, 10, 15–17]. Band gap modulation has been pursued by techniques such as doping with metals and non-metals, construction of heterojunctions by combining TiO2 with metals such as Pt or Pd, and other semiconductors such as MnO2, RuO2, and WO3, surface modifications, and size optimization. Techniques such as addition of quantum dots or dyes on the surface of TiO2 have been used to improve light sensitization [3, 5, 16].

Doping is carried out through the introduction of ions into the TiO2 matrix through various physical or chemical methods. This results in the introduction of impurity states within the bandgap, which contribute to the improved photocatalytic activity of TiO2 in various ways, such as either narrowing the bandgap, reduction of bulk recombination due to the increased charge traps that improve the separation of photocarriers, or by altering the conduction band position [10].

According to theoretical calculations, non-metal dopants mainly elevate the valence band edge to narrow the energy gap [18]. Photocatalytic improvement arising from non-metal doping has been attributed to various factors such as effective separation of photogenerated electron-hole pairs due to the shallow traps formed by the dopant states at the valence band edge, band gap narrowing due to the mixing of 2p orbitals of dopants such as N with O, and formation of defects arising from a charge compensation effect induced by the doping, bringing about the formation of a certain amount of oxygen vacancies and Ti3+ in TiO2 and a tail state in the band gap of TiO2, which favors more efficient utilization of incident light, leading to improved visible light activity [5, 10]. Trivalent dopants such as Ga and In have also shown a small red shift in the band gap of TiO2 which is attributed to the formation of oxygen vacancies [9].

Theoretical investigations reveal that transition metals mainly reduce the conduction band edge [18]. For transition metal dopants, such as Mn, V, and Cr, impurity states within the band gap are formed due to cation vacancies. Rare earth metal ion dopants improve the charge carrier separation efficiency, due to the 4f electrons, which act as a shallow trap for photogenerated electrons and holes [10]. However, there have been reports of higher visible light absorption without photocatalytic improvement with dopants such as Cr, while others reported an improvement above a critical Cr doping level [7]. This underscores the importance of other factors that affect photocatalytic performance of semiconductors such as their structural and morphological characteristics at the nanoscale, size, dimensionality, pore structure and volume, specific surface area, exposed surface facets, and crystalline phase content [10, 18].

Alkaline earth metallic dopants have been reported both from experimental and theoretical studies to improve the performance of anatase TiO2 in photocatalytic applications and perovskite solar cells due to shifting of the conduction and valence bands [6]. Non-toxic dopants such as alkaline earth metals would be suited for photocatalytic applications aimed at water treatment. Mg-doped TiO2 prepared using the mild sol-gel technique has been shown to have a mixed phase of anatase and rutile, with adequate photocatalytic activities under visible range of light [16]. Heterojunction photocatalysts, such as the anatase-rutile and anatase-brookite systems, have demonstrated superior visible light-induced photocatalytic activity [5].

Due to the mixed phase nature of TiO2 photocatalysts realized from experiments, more studies are required to further understand the effect of alkaline earth metal doping on the structural and electronic properties of the naturally occurring phases, rutile, anatase, and brookite TiO2. The orbital contributions of the wavefunctions at the valence band and conduction band edges can be a suitable method to provide clarity on the effect that alkaline earth metals have on TiO2 in general.

2. Computational Details

Density functional theory (DFT) calculations were carried out using the opEn-Source Package for Research in Electronic Structure, Simulation, and Optimization (Quantum ESPRESSO) package, which uses plane wave basis sets and pseudopotentials. The electronic wavefunctions were expanded in plane waves up to a cutoff energy of 40 Ry, while the core-valence interaction was treated using ultrasoft pseudopotentials (USPPs). The exchange-correlation was treated using the generalised gradient approximation (GGA), employing the Perdew–Burke–Ernzerhof (PBE) exchange-correlation functional (PBE-GGA). k-Point sampling used a (4 × 4 × 7) Monkhorst–Pack sampling grid for the bulk unit cells to carry out the integration using the linear tetrahedron method with Bloechl's corrections over the irreducible Brillouin zone and the Marzari–Vanderbilt smearing scheme with a Gaussian spreading of 0.05 Ry. Electronic ground state energy was calculated through self-consistent cycles together with numerical methods such as Davidson iterative diagonalization schemes for evaluation of the solution to the Kohn–Sham equation. The iterations ended at a convergence criterion of 10–8 eV. The maximum number of geometric and electronic iterations was set at 100. Generally, all calculations began from scratch for geometry optimization and electronic property calculations. The Visualization for Electronic Structural Analysis (VESTA) visualization software was used to realize the TiO2 unit and supercells and to obtain the atomic positions. Optimization of the bulk structures was carried out, starting with experimental lattice parameters. 2 × 2 × 1 supercells, having 4-unit cells each, were then constructed. The number of atoms in each supercell is 48, 24, and 96, for anatase, rutile, and brookite, respectively. Mg (Ca) mono-doped TiO2 models were realized by single cationic substitution of one Mg (Ca) atom for one Ti atom. The substitution site is chosen based on X-ray diffraction data, which establish that Mg occupies a lattice Ti site [6]. Hence, the obtained configuration is Ti(15)XO(32), Ti(31)XO(64), and Ti(7)XO(16), where X □ Mg(Ca), representing 2.08 at%, 1.00 at%, and 4.16 at% doping concentrations for anatase, brookite, and rutile, respectively. After atomic substitution, both atomic positions and cell

parameters of doped models were relaxed until the residual forces were below 10–03 Ry/Bohr.

3. Results and Discussion

In this section, the structural and electronic properties of doped and undoped anatase, brookite, and rutile will be discussed. The results for structural optimization of the unit cells for the three polymorphs from which the 2 × 2 × 1 supercells were constructed from will first be discussed, followed by the structural properties of the Mg(Ca)-doped polymorphs. The electronic properties of the undoped and doped polymorphs will then be discussed.

3.1. Structural Optimization. Figure 1 shows the unit cells of anatase, brookite, and rutile as modelled using VESTA visualization software, consisting of TiO6 octahedra, where a Ti atom binds with six O atoms.

The unit cells consist of 4 titanium (Ti) and eight oxygen (O) atoms, 8 Ti and 16 O atoms, and 2 Ti and 4 O atoms for anatase, brookite, and rutile, respectively.

To optimize the tetragonal structures of anatase and rutile, minimization with respect to the lattice parameter a was carried out at a constant c/a ratio. For anatase, the optimized lattice constant of $a = 7.22$ Bohr $= 3.821$ Å was obtained as shown in Figure 2. Fixing the lattice parameter a at the optimized value, minimization was carried out at varying c/a ratios. The optimal ratio of 2.58 was obtained as shown in Figure 2. The optimized cell parameters for pure anatase TiO2 are therefore $a = b = 3.821$ Å c $= 9.856$ Å, which is comparable to the results of Ma et al. of $a = b = 3.796$ Å c $= 9.722$ Å , also obtained using the GGA approximation with a 2 × 2 × 1 supercell [6].

The lattice parameters obtained in this work agree well with other theoretical [3, 6, 8, 19, 20] and experimental results [6, 8, 21]. The optimal lattice parameter obtained for rutile is $a = 8.7$ Bohr $= 4.603$ Å and a c/a ratio of $c/a = 0.65$. The optimized cell parameters for pure rutile TiO2 are therefore $a = b = 4.603$ Å c $= 2.992$ Å , which are in good agreement with other theoretical [15, 19, 22–25] and experimental values [19, 21], including those obtained using the full-potential linearized augmented plane-wave method (FP-LAPW), employing the GGA exchange-correlation functional [19], showing the reliability of our method. The optimized lattice parameter of brookite is $a = 17.44$ Bohr $= 9.234$ Å. The b/a and c/a ratios are 0.599 and 0.554, respectively. These results are quite comparable to those from other theoretical [20, 26] and experimental studies [20, 27].

The optimized lattice parameters for brookite are therefore $a = 9.234$ Å, $b = 5.530$ Å, and $c = 5.116$ Å.

From the optimized bulk unit cells, 2 × 2 × 1 supercells were constructed, each consisting of 4 unit cells, having 48, 96, and 24 atoms for anatase, brookite, and rutile, respectively, as shown in Figure 4.

Single cationic substitution of Mg(Ca) was carried out into the Ti site of the supercells of the three polymorphs as shown in Figure 4(d) for anatase.

After atomic and lattice parameter relaxation, optimization of the supercells was carried out. In general, the lattice parameters of the doped systems are proportional to the dopant ionic radius and increase in the order of undoped TiO2 ⟶ Mg-doped ⟶ Ca-doped, as expected. This is more obvious in the case of the tetrahedral structures, compared to the orthorhombic brookite structure, in which, even though an increase in volume with both dopants is noted, the increase is very slight with Mg doping due to its smaller ionic radius compared to Ca as shown in Table 1. This indicates that the introduction of the dopant causes volume expansion.

The reduced volume expansion in brookite can be attributed to the symmetry of the orthorhombic unit cell, which influences the extent of the interaction between the orbitals upon doping. Bonding in Ti–O is described as having both a covalent and ionic character, arising from hybridization between Ti 3d and O 2p orbitals on one hand and from charge transfer between Ti and O on the other hand, respectively, resulting in the formation of Ti with varying charges [28, 29]. The covalent nature increases as the charge on Ti increases, in the order of Ti2+ ⟶ Ti3+ ⟶ Ti4+ and with an associated decrease in the ionic radii in the same order [29]. We infer that doping with Mg and Ca in brookite causes an increase in the covalent nature of the Ti–O bond in the orthorhombic brookite structure, arising from the substitution of a Ti atom with a divalent dopant ion.

As is evident from Figure 5, the doped rutile structures are more energetically stable than the pure rutile, with Mg rutile being most stable.

3.2. Electronic Properties. In this section, a detailed description of the orbital nature of the wave functions at the valence and conduction band edges of the TiO2 polymorphs will be provided. This is critical in the understanding of modification of its electronic structure through the introduction of impurities. In order to study the doping mechanism, the total density of states (TDOS) and projected density of states (PDOS) of pure and doped TiO2 polymorphs will be discussed. Figure 6 represents the TDOS and PDOS of both rutile and brookite polymorphs of TiO2, while TDOS of anatase is shown in Figure 7.

The valence band edge for rutile lies higher than that of anatase and brookite and it comprises mainly of O-2p states, while the conduction band edge comprises mainly of Ti- 3d states in the three cases, in agreement with previous reports on the orbital nature of the wave functions near the valence edge of TiO2 [10].

Figure 7(a) shows the band structure of anatase before doping. As is evident from Figure 7(b), introduction of dopant states results in a shift of the valence band edge to higher energies in both cases of Mg and Ca doping of anatase TiO2, with the increase of the valence band edge being more prominent with Ca doping.

This effect is clearly seen from the band structure diagrams. Figure 8 shows the increase of the valence band edge to higher energies in brookite, upon doping with Mg, which

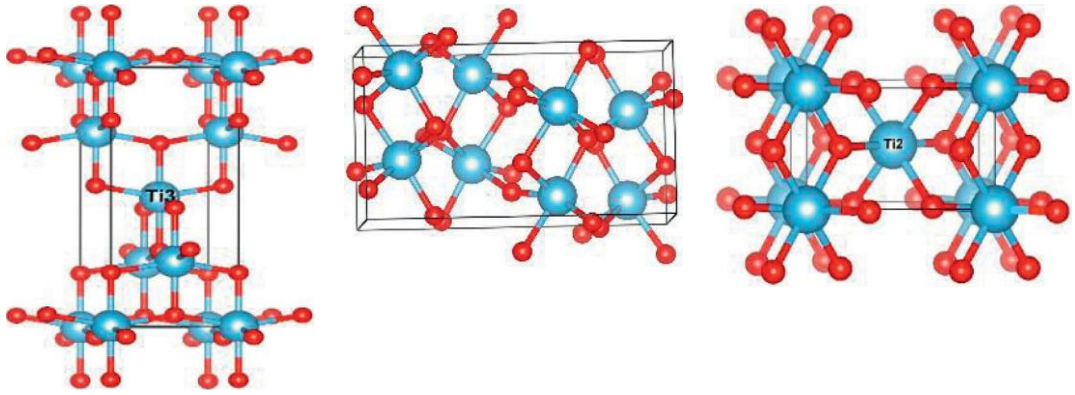

(a) (b) (c)

FIGURE 1: Bulk unit cells for (a) 12 atom tetragonal anatase (space group 141/amd), (b) 24 atom orthohormbic brookite (space group pbca), and (c) 6 atom tetragonal rutile (space group P42/mnm).

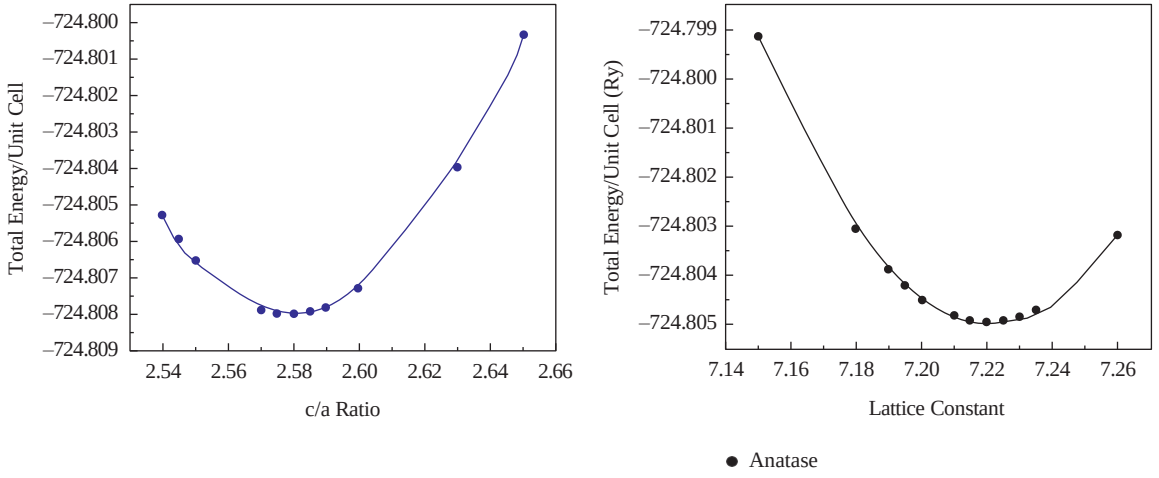

(a) (b)

FIGURE 2: (a) **c**/**a** ratio optimization and (b) lattice parameter **a** optimization at **c**/**a** □ 2.58 of anatase unit cell.

occurred for all the polymorphs upon doping with either Mg or Ca.

Figure 9 illustrates the PDOS of the Mg and Ca dopant states in brookite. It is evident that the Ca states are of higher energies and are closer to the edge of the valence band, compared to Mg dopant states.

The result of this is that there are intra-band Mg *p* and *s* states which are of sufficiently low localized energy levels to lie at the top of the valence band as shown in Figure 9(a), while Ca causes the formation of both intra-band and inter-band (mid-gap states), by pushing the valence band maximum to higher energies, slightly above the Fermi level as shown in Figure 9(b). Similar to N doping, the mixing of dopant and O 2p orbitals leads to band gap narrowing [5], with the effect being most pronounced in anatase compared to rutile and brookite from the results of this study. This observation would have implications on the performance of the doped TiO2 as a photocatalyst.

One of the consequences that would arise from the introduction of dopant states is trapping of photogenerated electrons and holes, which would lead to the separation of the carriers from the bands. This would reduce charge recombination, allowing the carriers to successfully diffuse to the surface, hence improving the photocatalytic effect as explained in literature [30]. Additionally, by substituting Ti with Mg (Ca), two holes per single dopant ion are injected into the system, resulting in impurity band states arising from isolated O 2p states above the valence band maximum [31]. This effect is well observed in this work, with the O 2p isolated tail states appearing more prominently in the case of Ca doping for the case of anatase, while the valence band is fully occupied in pure anatase as shown in Figure 10.

Similar to Sn doping, the Ca states lie above the valence band and could act as trapping sites for holes. This effect was observed to cause Sn-doped TiO2 to exhibit enhanced visible light region photocatalytic activity compared to undoped TiO2 in dye degradation experiments [30].

The calculated band gaps are 2.10 eV, 1.8 eV, and 2.35 eV for anatase, rutile, and brookite, respectively. The values are compared favorably with other theoretical values such as

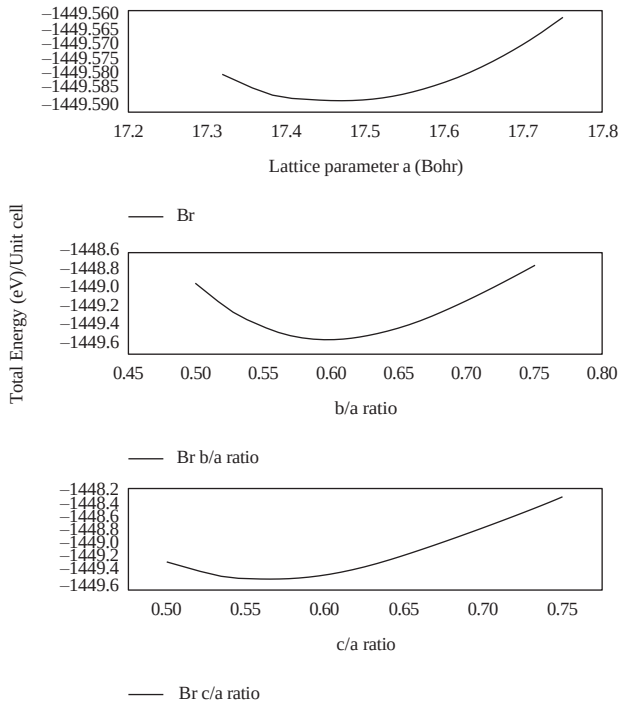

FIGURE 3: Structural optimization of brookite.

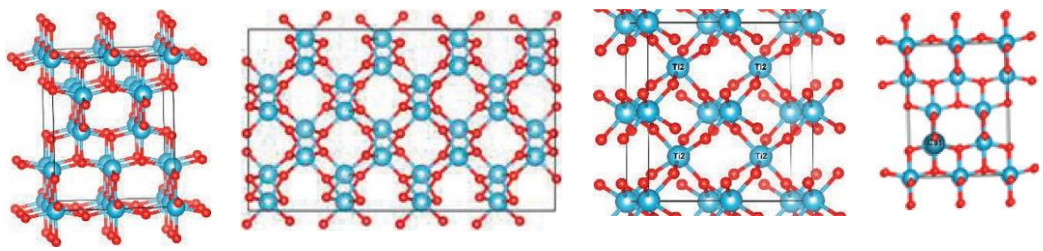

FIGURE 4: 2 × 2 × 1 supercells of (a) 48-atom anatase, (b) 96-atom brookite, and (c) 24-atom rutile. (d) Single cationic substitution at Ti site in anatase supercell. Ti atoms are represented by light blue circles, and O atoms are represented by red circles.

TABLE 1: The optimized structural parameters of pure and doped polymorphs.

Configuration	a (Å)	b (Å)	c (Å)
Pure anatase	3.820	3.820	9.857
Mg-doped anatase	3.840	3.840	9.988
Ca-doped anatase	3.930	3.930	10.660
Pure brookite	9.234	5.540	5.116
Mg-doped brookite	9.207	5.524	5.156
Ca-doped brookite	9.247	5.548	5.179
Pure rutile	4.603	4.603	2.992
Mg-doped rutile	4.736	4.736	3.221
Ca-doped rutile	4.974	4.974	3.730

2.17 eV [6] and 2.04 eV [26] for anatase, 1.86 eV [20], 1.87 eV [15], and 1.78 V [26] for rutile and 2.20 eV [26] and 2.38 eV [20] for brookite. Doping with Mg(Ca) raises the valence band maximum in all the cases, with a negligible effect on the conduction band minimum. This causes a reduction in the band gap, of 0.2 eV for anatase and rutile and 0.1 eV for brookite for single cationic substitution. It is noted that the least reduction in band gap is exhibited in brookite with the

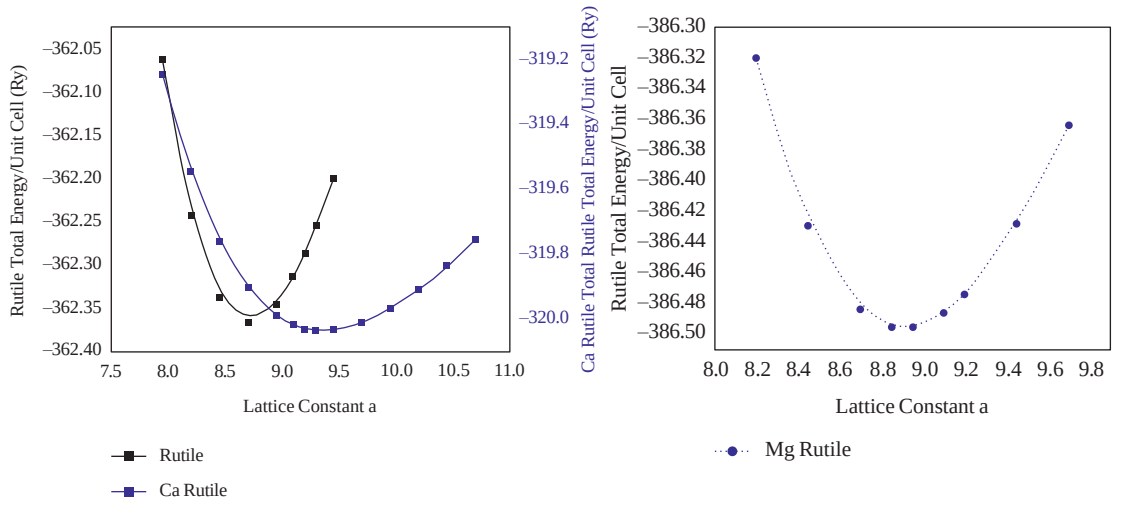

FIGURE 5: Total energy vs. lattice constants of pure and doped rutile.

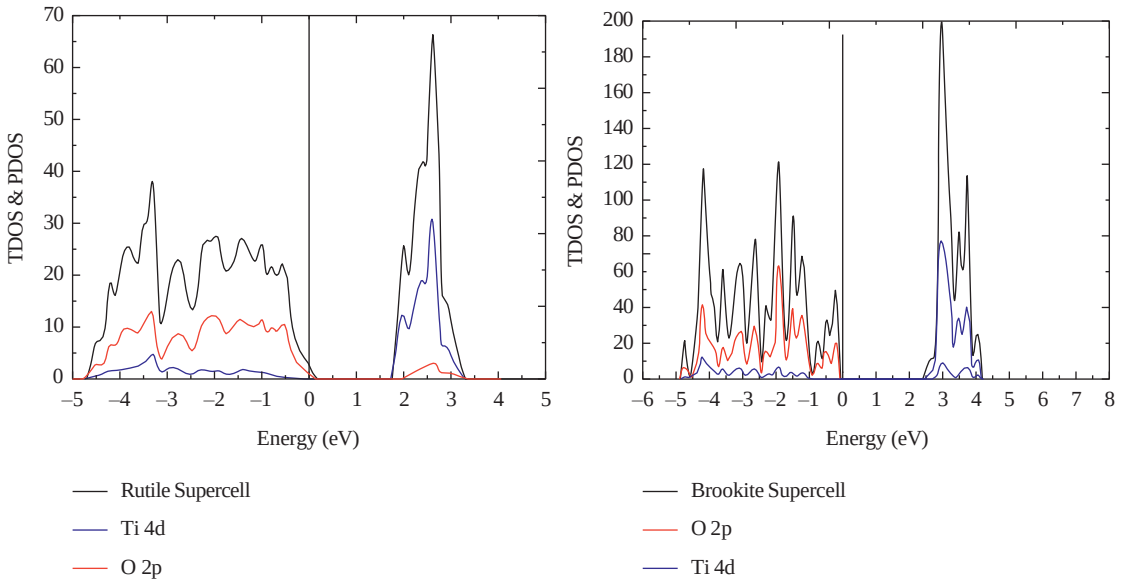

FIGURE 6: TDOS and PDOS of pure rutile and brookite.

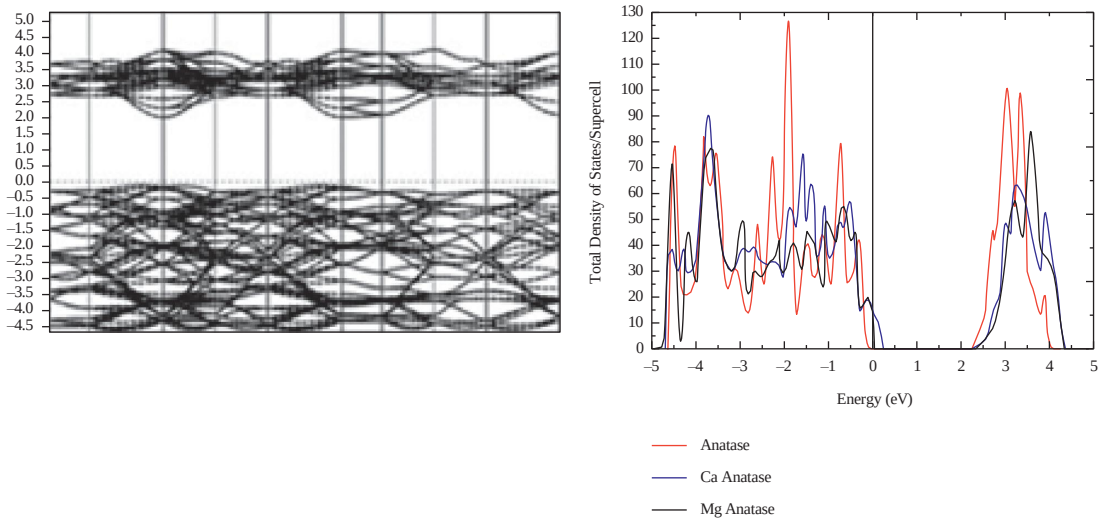

(a) (b)

FIGURE 7: (a) Anatase band structure and (b) TDOS and PDOS of doped and undoped anatase.

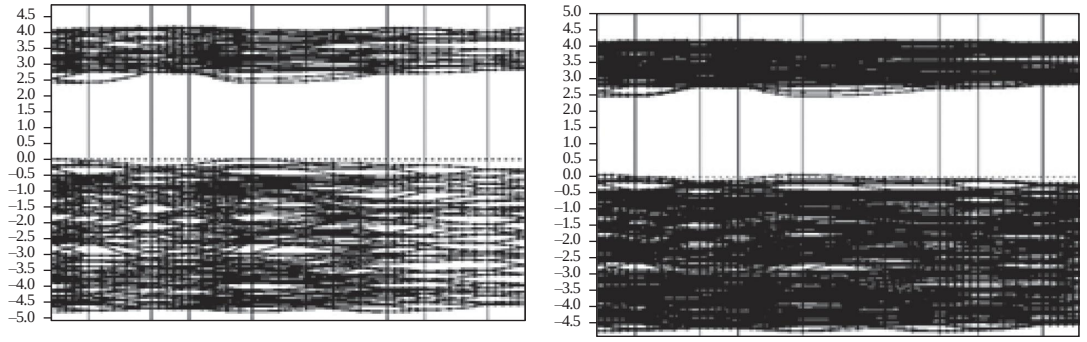

(a) (b)

FIGURE 8: Band structures for (a) brookite and (b) Mg-doped brookite.

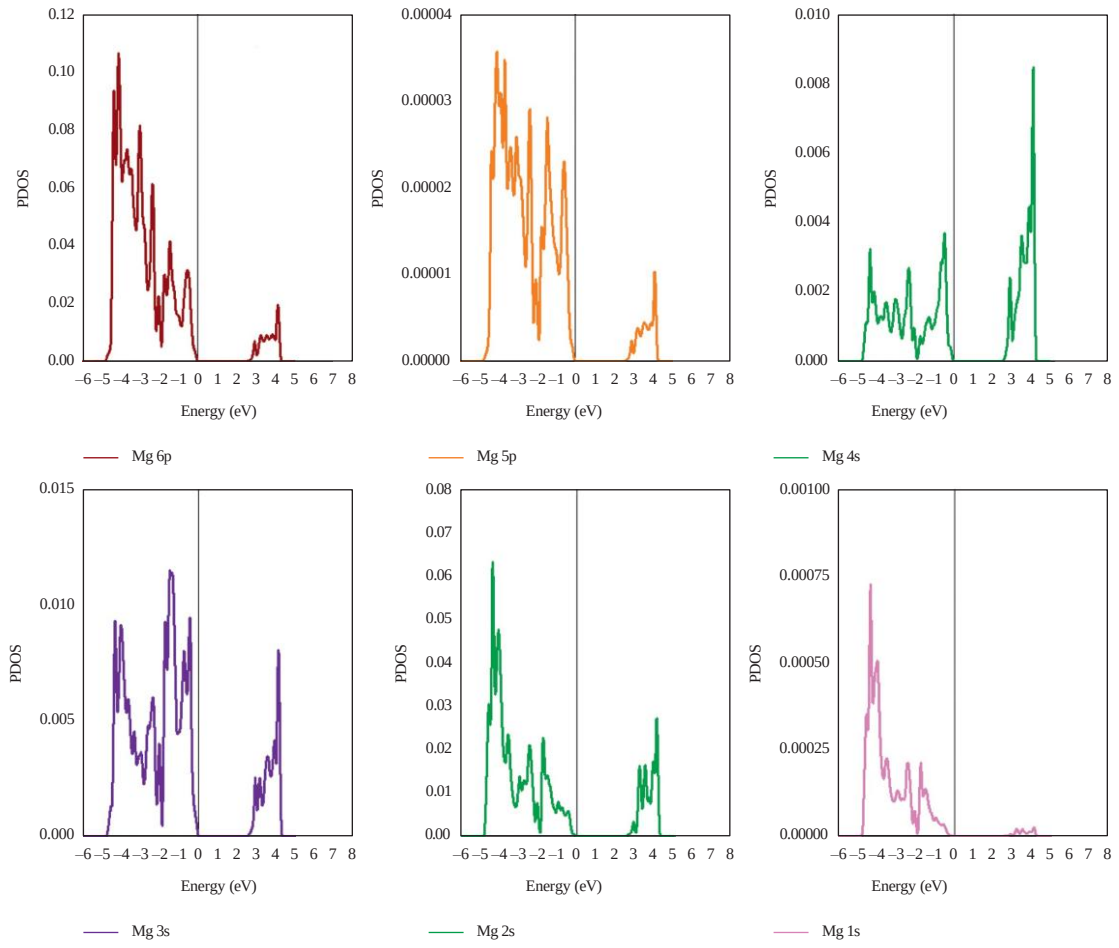

(a)

FIGURE 9: Continued.

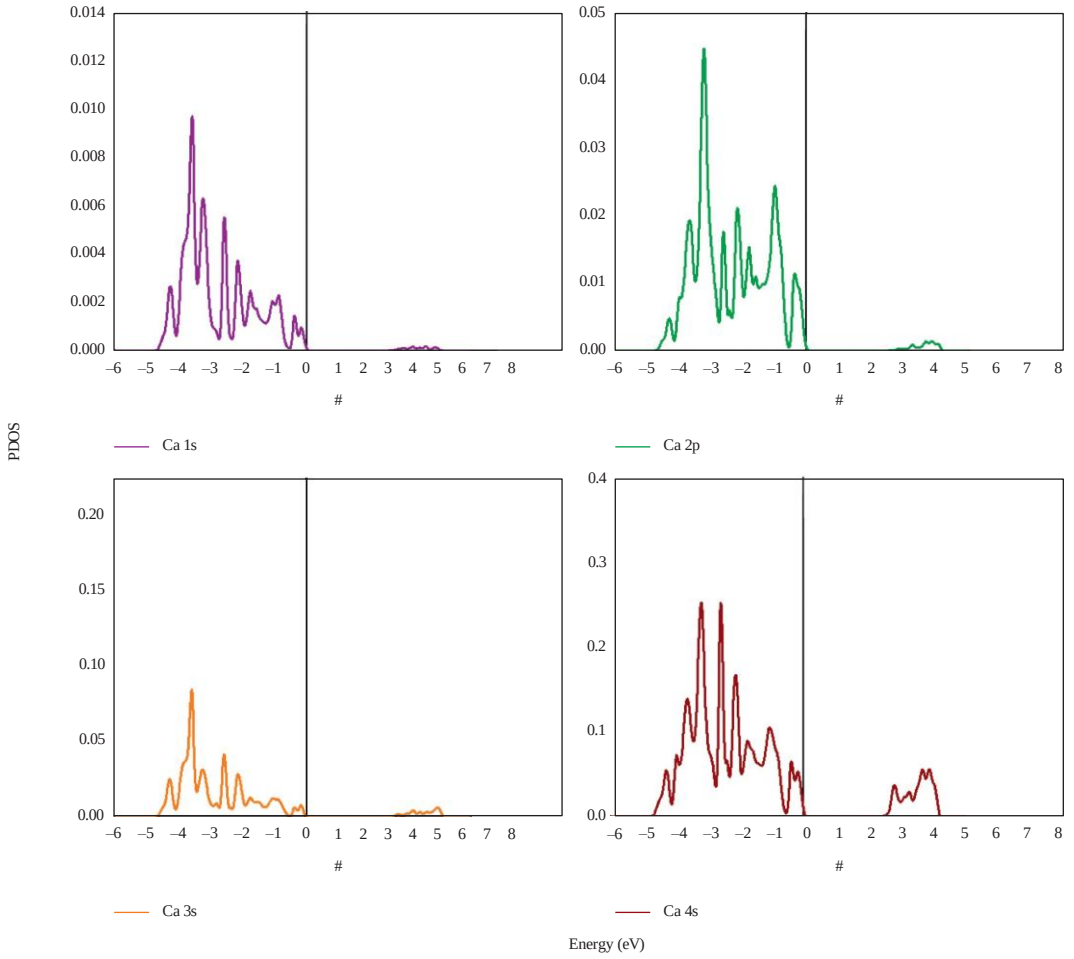

(b)

Figure 9: (a) Mg dopant states and (b) Ca dopant states in brookite.

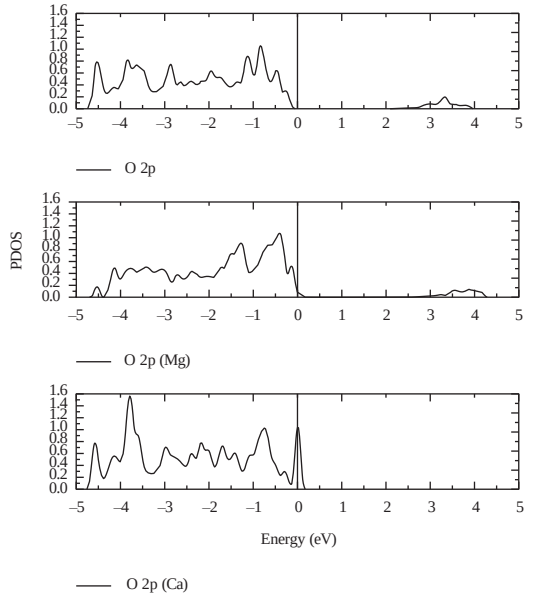

Figure 10: PDOS of O 2p states in anatase.

lowest doping concentration, pointing to the importance of crystalline phase and doping concentration in band gap tuning.

4. Conclusion

Doping of titania with Mg and Ca dopant ions leads to the reduction of the band gap energy due to the mixing of dopant and O 2p orbitals, an effect normally mostly observed with non-metal doping such as with N. Intra and inter-band states are formed at the edge of the valence band minimum. A tail state is observed in the band gap of TiO2 upon doping, as a result of oxygen vacancy defects arising from charge compensation. These electronic structure modifications which are most pronounced in the anatase crystalline phase would be favorable for photocatalytic improvement, through factors such as effective separation of photogenerated electron-hole pairs and more efficient utilization of incident light.

Data Availability

The data that support the findings of this study are available from the corresponding author upon reasonable request.

Conflicts of Interest

The authors declare that they have no conflicts of interest.

Acknowledgments

The Centre for High Performance Computing (CHPC) in South Africa is gratefully acknowledged for providing the computational resources used in this work.

References

[1] W. Zeng, T. Liu, Z. Wang, S. Tsukimoto, M. Saito, and Y. Ikuhara, "Oxygen adsorption on anatase TiO2 (101) and (001) surfaces from first principles," *Materials Transactions*, vol. 51, no. 1, pp. 171–175, 2010.

[2] H. Sutrisno and Sunarto, "Synthesis of TiO2-polycrystalline microspheres and its microstructure at various high temperatures," *Journal of Ceramic Processing Research*, vol. 18, pp. 378–384, 2017.

[3] Y. Wang, R. Zhang, J. Li, L. Li, and S. Lin, "First-principles study on transition metal-doped anatase TiO2," *Nanoscale Research Letters*, vol. 9, no. 1, p. 46, 2014.

[4] J. Lu, H. Jin, Y. Dai, K. Yang, and B. Huang, "Effect of electronegativity and charge balance on the visible-light-responsive photocatalytic activity of nonmetal doped anatase TiO2," *International Journal of Photoenergy*, vol. 2012, Article ID 928503, 2011.

[5] R. Fagan, D. E. McCormack, D. D. Dionysiou, and S. C. Pillai, "A review of solar and visible light active TiO2 photocatalysis for treating bacteria, cyanotoxins and contaminants of emerging concern," *Materials Science in Semiconductor Processing*, vol. 42, pp. 2–14, 2016.

[6] J.-G. Ma, C.-R. Zhang, J.-J. Gong et al., "The electronic structures and optical properties of alkaline-earth metals doped anatase TiO2: a comparative study of screened hybrid functional and generalized gradient approximation," *Materials*, vol. 8, no. 8, pp. 5508–5525, 2015.

[7] G. C. Va´squez, D. Maestre, A. Cremades et al., "Understanding the effects of Cr doping in rutile TiO2 by DFT calculations and X-ray spectroscopy," *Scientific Reports*, vol. 8, no. 1, Article ID 8740, 2018.

[8] R. Long and N. J. English, "Density functional theory studies of doping in titania," *Molecular Simulation*, vol. 36, no. 7-8, pp. 618–632, 2010.

[9] A. Iwaszuk and M. Nolan, "Charge compensation in trivalent cation doped bulk rutile TiO2," *Journal of Physics: Condensed Matter*, vol. 23, no. 33, Article ID 334207, 2011.

[10] X. Kang, S. Liu, Z. Dai, Y. He, X. Song, and Z. Tan, "Titanium dioxide: from engineering to applications," *Catalysts*, vol. 9, no. 2, pp. 191–2, 2019.

[11] R. Sun, Z. Wang, M. Saito, N. Shibata, and Y. Ikuhara, "Atomistic mechanisms of nonstoichiometry-induced twin boundary structural transformation in titanium dioxide," *Nature Communications*, vol. 6, no. 1, Article ID 7120, May 2015.

[12] C. E. Ekuma and D. Bagayoko, "Ab-initioElectronic and structural properties of rutile titanium dioxide," *Japanese Journal of Applied Physics*, vol. 50, no. 10, Article ID 101103, 2011.

[13] Z. Wang, W. Zeng, L. Gu, M. Saito, S. Tsukimoto, and Y. Ikuhara, "Atomic-scale structure and electronic property of the LaAlO3/TiO2 interface," *Journal of Applied Physics*, vol. 108, no. 11, Article ID 113701, 2010.

[14] H. C. Wu, Y. S. Lin, and S. W. Lin, "Mechanisms of visible light photocatalysis in N-doped anatase TiO2with oxygen vacancies from GGA+U calculations," *International Journal of Photoenergy*, vol. 2013, pp. 1–7, Article ID 289328, 2013.

[15] H. Chen, X. Li, R. Wan, S. Kao-Walter, and Y. Lei, "A DFT study of the electronic structures and optical properties of (Cr, C) co-doped rutile TiO2," *Chemical Physics*, vol. 501, pp. 60–67, 2018.

[16] H. P. Shivaraju, G. Midhun, K. M. Anil Kumar, S. Pallavi, N. Pallavi, and S. Behzad, "Degradation of selected industrial dyes using Mg-doped TiO2 polyscales under natural sun light as an alternative driving energy," *Applied Water Science*, vol. 7, no. 7, pp. 3937–3948, 2017.

[17] M. Devi and M. R. Panigrahi, "Synthesis and characterization of Mg doped TiO2 thin film for solar cell application," *International Journal of Engineering and Applied Sciences*, vol. 7, no. 2, p. 1, 2015.

[18] J. Zhang, L. Qian, W. Fu, J. Xi, and Z. Ji, "Alkaline-earth metal Ca and N codoped TiO2 with exposed {001} facets for enhancing visible light photocatalytic activity," *Journal of the American Ceramic Society*, vol. 97, no. 8, pp. 2615–2622, 2014.

[19] A. Rubio-Ponce, A. Conde-Gallardo, and D. Olgu´ın, "First-principles study of anatase and rutileTiO2doped with Eu ions: a comparison of GGA andLDA+Ucalculations," *Physical Review B*, vol. 78, no. 3, Article ID 035107, 2008.

[20] J. Zhang, P. Zhou, J. Liu, and J. Yu, "New understanding of the difference of photocatalytic activity among anatase, rutile and brookite TiO2," *PCCP: Physical Chemistry Chemical Physics*, vol. 16, no. 38, pp. 20382–20386, 2014.

[21] J. K. Burdett, T. Hughbanks, G. J. Miller, J. W. Richardson, and J. V. Smith, "Structural-electronic relationships in inorganic solids: powder neutron diffraction studies of the rutile and anatase polymorphs of titanium dioxide at 15 and 295 K," *Journal of the American Chemical Society*, vol. 109, no. 12, pp. 3639–3646, 1987.

[22] J. Muscat, N. M. Harrison, and G. Thornton, "Effects of exchange, correlation, and numerical approximations on the computed properties of the rutileTiO2(100) surface," *Physical Review B*, vol. 59, no. 3, pp. 2320–2326, 1999.

[23] H. Liu, G. Liu, and Q. Zhou, "Preparation and characterization of Zr doped TiO2 nanotube arrays on the titanium sheet and their enhanced photocatalytic activity," *Journal of Solid State Chemistry*, vol. 182, no. 12, pp. 3238–3242, 2009.

[24] P. J. D. Lindan, N. M. Harrison, M. J. Gillan, and J. A. White, "First-principles spin-polarized calculations on the reduced and reconstructedTiO2(110) surface," *Physical Review B*, vol. 55, no. 23, p. 15919, 1997.

[25] Z. L. Zeng, "First-Principles study on the structural and electronic properties of N atoms doped-rutile TiO2of oxygen vacancies," *Advances in Materials Science and Engineering*, vol. 2015, pp. 1–10, 2015.

[26] S.-D. Mo and W. Y. Ching, "Electronic and optical properties of three phases of titanium dioxide: rutile, anatase, and brookite," *Physical Review B*, vol. 51, no. 19, pp. 13023–13032, May 1995.

[27] E. P. Meagher and G. A. Lager, "Polyhedral thermal expansion in the TiO2 polymorphs; refinement of the crystal structures of rutile and brookite at high temperature," *The Canadian Mineralogist*, vol. 17, pp. 77–85, 1979.

[28] B. Jiang, J. M. Zuo, N. Jiang, M. O'Keeffe, and J. C. H. Spence, "Charge density and chemical bonding in rutile, TiO2," *Acta Crystallographica Section A Foundations of Crystallography*, vol. 59, no. 4, pp. 341–350, 2003.

[29] C. Sousa and F. Illas, "Ionic-covalent transition in titanium oxides," *Physical Review B*, vol. 50, no. 19, pp. 13974–13980, 1994.

[30] F. Huang, A. Yan, and H. Zhao, *Influences of Doping on Photocatalytic Properties of TiO2 Photocatalcyst*, intechopen, London, UK, 2016.

[31] Y. Liu, W. Zhou, and P. Wu, "Room-temperature ferromagnetism and optical properties in Mg-doped TiO2: a density functional theory investigation," *Journal of Applied Physics*, vol. 115, no. 12, Article ID 123913, 2014.